Microporous and Mesoporous Materials 124 (2009) 197–203

Contents lists available at ScienceDirect

Microporous and Mesoporous Materials

journal homepage: www.elsevier.com/locate/micromeso

Preparation and characterization of highly active mesoporous TiO_2 photocatalysts by hydrothermal synthesis under weak acid conditions

Jikai Liu [a,c], Taicheng An [a,*], Guiying Li [a], Ningzhong Bao [b], Guoying Sheng [a], Jiamo Fu [a]

[a] State Key Laboratory of Organic Geochemistry and Guangdong Key Laboratory of Environmental Resources Utilization and Protection, Guangzhou Institute of Geochemistry, Chinese Academy of Sciences, No. 511, Kehua Street, Tianhe Dict., Guangzhou 510640, China
[b] Center for Materials for Information Technology, The University of Alabama, Tuscaloosa, AL 35487, USA
[c] Graduate School of Chinese Academy of Sciences, Beijing 100049, China

ARTICLE INFO

Article history:
Received 20 October 2007
Received in revised form 2 February 2009
Accepted 6 May 2009
Available online 13 May 2009

Keywords:
Mesoporous TiO_2
Preparation
Hydrothermal treatment
Acetic acid
Photocatalytic activity

ABSTRACT

Mesoporous TiO_2 photocatalysts have been synthesized in acetic acid aqueous solutions by using the amphiphilic triblock copolymer (Pluronic P123) template. The prepared photocatalysts were characterized by means of X-ray diffraction, transmission electron microscopy and nitrogen adsorption/desorption analysis. The phase and structural qualities of the obtained mesoporous TiO_2 have been improved by using hydrothermal treatment. The hydrolysis reaction of titanium sources has been controlled by using a low concentrated acetic acid aqueous solution used as both hydrolytic retardants and acid catalysts because of the strong chelating effect and acidity of acetic acid. The obtained mesoporous TiO_2 exhibits uniform mesoporous structure with different mean pore sizes of up to 9.0 nm. The photocatalytic activity of the obtained photocatalysts was investigated, using dimethyl phthalate as a modal pollutant. Over 90% of dimethyl phthalate can be photocatalytically degraded within 2 h under UV irradiation in the presence of the obtained photocatalysts with a concentration of 2 g/L. The calcination temperature is the most remarkable factor that can affect the ultimate photocatalytic activity of the prepared photocatalysts.

1. Introduction

The discovery of the surfactant-templated self-assembly of mesoporous SiO_2 in the early 1990s [1,2] has triggered extensive research on ordered mesoporous transition metal oxides because of the potential application in fields of catalysis [3–5], separation technology [6,7], polymerization [8] and nanoelectronics [9]. Mesoporous TiO_2 (M-TiO_2) has received considerable attention because of the distinguished mesostructure and the outstanding photocatalytic activity for the complete destruction and elimination of organic contaminants in the environment [10]. Hence, various strategies have been developed to successfully synthesize M-TiO_2 [11–16].

Surfactant templates, such as ionic [14,15] and neutral surfactants [16–20], have been widely used to synthesize mesoporous materials based on different organic–inorganic interactions including electrostatic [21,22], hydrogen bonding [17], etc. However, the unchangeable intrinsic structure of the surfactant templates cannot manipulate the mesostructure of synthesized samples. Recently, amphiphilic triblock copolymers have been increasingly employed to organize mesostructured composite solids [23–28], in which the architecture of the synthesized products are able to be continuously tuned by adjusting the synthetic conditions such as the ratio of surfactant to inorganic species, the molecular weight of surfactant, etc. [29]. However, the synthesis of M-TiO_2 is still challengeable due to the rapid hydrolysis of titanium sources, and thus the strong acid catalyst (HCl and HNO_3) and ligand complexation (acetylacetone, oxalate and citrate) are conventionally used in the synthesis. Most of the used hydrolytic retardants are strongly corrosive and toxic. In addition, the photooxidation activity of the obtained photocatalysts declines because of the introduction of a certain amount of inorganic ions, in particularly the Cl^- in HCl solution [30]. Acetic acid aqueous solution (HAc-AS), however, is a particularly interesting candidate as a typical nontoxic and environmental-friendly organic acid with small molecular weight and strong chelating effect. Conventionally, acetic acid has been adopted to control the hydrolysis of titanium sources based on the slow release of water through the esterification reaction between acetic acid and alcohols [31–33]. However, the strong chelating effect of acetic acid [34,35] has been pitifully neglected in the synthesis of M-TiO_2. Quite recently, Yu et al. [36] has successfully prepared M-TiO_2 ultrasonically by employing acetic acid as a modifying agent to slow down the hydrolysis rate and directly introducing water from the environment. However, the obtained M-TiO_2 exhibits a H3 hysteresis loop and a relatively small mean pore size (about 4 nm) [36], which may inevitably confine its potential applications. Moreover, no studies have been devoted to

* Corresponding author. Tel.: +86 20 85291501; fax: +86 20 85290706.
E-mail address: antc99@gig.ac.cn (T. An).

1387-1811/$ - see front matter © 2009 Elsevier Inc. All rights reserved.
doi:10.1016/j.micromeso.2009.05.009

systematically investigating the performance of weak acid solutions, e.g. HAc-AS, in controlling the hydrolysis of titanium sources.

In the present work, large-pore M-TiO_2 with narrow pore size distributions have been prepared for the purposes of less experimental pollution, time saving, improved structural qualities and enhanced photocatalytic activity using a hydrothermal-assisted sol–gel method at low concentrated HAc-AS used as hydrolytic retardants. Importantly, as the advantages of non-ionic surfactants in organizing the structure of the material and creating well-defined and reproducible nanophases [32], Pluronic P123 was used to direct the formation of mesophases. The influence factors, such as the concentration of HAc-AS, the time of hydrothermal treatment and the calcination temperature, were investigated in detail in order to tune the textures of the synthesized photocatalysts. The photocatalytic activities of the prepared M-TiO_2 were evaluated by using dimethyl phthalate (DMP) as a model organic pollutant.

2. Experimental

2.1. Preparation of M-TiO_2

M-TiO_2 was prepared using the hydrothermal-assistant sol–gel method. In a typical synthesis, 5 g titanium butoxide (M = 340.36, 98%, $Ti(OC_4H_9)_4$) was added dropwise to 30 mL HAc (A.R.) aqueous solution under vigorous stirring. The mixed solution was sealed and kept stirring for 4 h to obtain solution A. In order to investigate the effect of the HAc-AS concentration, 10%, 20%, 40% and 80% (v/v) HAc-AS were adopted, respectively. In a separated beaker, 3 g block copolymer $HO(CH_2CH_2O)_{20}(CH_2CH(CH_3)O)_{70}(CH_2CH_2O)_{20}H$ (Mav = 5800, purchased from Aldrich, designated $EO_{20}PO_{70}EO_{20}$, Pluronic P123) was dissolved in 20 mL ethanol (A.R.) thoroughly under vigorous stirring to obtain solution B. Solution B was then slowly added to solution A. The final solution mixture was sealed and further stirred for 24 h. All the above experiments were conducted at room temperature. The solution was then transferred into a Teflon sealed container which was then heated in an oven at 120 °C for 24, 48 and 72 h, respectively. After reaction, the precipitation was collected and dried in air at 80 °C overnight without further washing. The as-prepared samples were finally calcined at different temperatures of 300, 450, 600 and 750 °C for 4 h to remove organic surfactants and improve the crystallinity of the products. The M-TiO_2 prepared by hydrothermal treatment for 48 h in 20% HAc-AS and then calcined at 450 °C was designated as representative sample for comparison. Deionized and doubly distilled water was used throughout the experiment.

2.2. Characterization of M-TiO_2

The crystal phase, phase composition and crystallinity of the obtained M-TiO_2 was determined by X-ray diffractometer (Rigaku D/MAX-2200 VPC) with Cu Kα radiation (λ = 0.15418 nm) at an accelerating voltage of 40 kV, an emission current of 30 mA and a scanning speed of 5°/min. The morphology was observed using transmission electron microscopy (TEM, Jeol JEM-100CXII) with an accelerating voltage of 100 kV. Nitrogen adsorption and desorption isotherms were obtained at 77 K with a Micromeritics ASAP 2010 system.

2.3. Characterization of photocatalytic activity

Photocatalytic experiments were performed in aqueous solutions containing DMP (A.R.) with an initial concentration of 2.5×10^{-4} mol/L. The photocatalytic reactor consists of a 160 mL Pyrex glass bottle with a jacket outside and a 125 W high pressure Hg lamp in parallel to the Pyrex glass bottle. In all the experiments, the reaction temperature was kept at 27 ± 2 °C by a continuous circulation of water in the jacket around the reactor. Reaction suspensions were prepared by adding different amount of the photocatalyst powders to 150 mL DMP aqueous solution under vigorous stirring. Prior to irradiation, all the reaction suspensions were kept on stirring in dark for 30 min to establish an adsorption–desorption equilibrium. The reaction time was counted as the Hg lamp was turned on. A small amount of the reaction suspension was taken out at given time intervals, and filtered through a 0.2 μm Millipore filter. The photocatalysts were maintained in suspension using magnetic stirring.

2.4. Analysis methods

The concentrations of DMP in the suspensions were monitored by an Agilent 1200 high pressure liquid chromatography (HPLC) equipped with a UV detector (λ = 225 nm). After injecting 20 μL of samples, the substances were separated by a NUCLEODUR 100-5 C18 reverse-phase column (150 mm × 4.6 mm, 5 μm). The mobile phase consisted of 40 vol.% water and 60 vol.% acetonitrile pumped at 0.6 mL/min. The column was thermostated at 30 °C. The chromatographic areas of experimental samples were converted to the concentration values using calibration curves based on the standard compounds.

3. Results and discussion

3.1. Characterization of prepared M-TiO_2

3.1.1. XRD analysis

The wide-angle XRD patterns of the obtained M-TiO_2 are presented in Figs. 1–3. Table 1 shows the mean crystal sizes of the obtained M-TiO_2 calculated by the Scherrer formula [37]. The main diffraction peaks are indexed as the (1 0 1), (0 0 4), (2 0 0), (1 0 5), (2 1 1), (2 0 4) and (1 1 6) reflections of crystalline anatase phase, corresponding to those shown in the JCPDS card No. 21-1272. No reflections of rutile and brookite phases are observed in the prepared M-TiO_2. As shown in Fig. 1, with increasing the concentration of HAc-AS, the diffraction peak intensity becomes stronger and the peak width becomes narrower, which reveals that the grain sizes become larger.

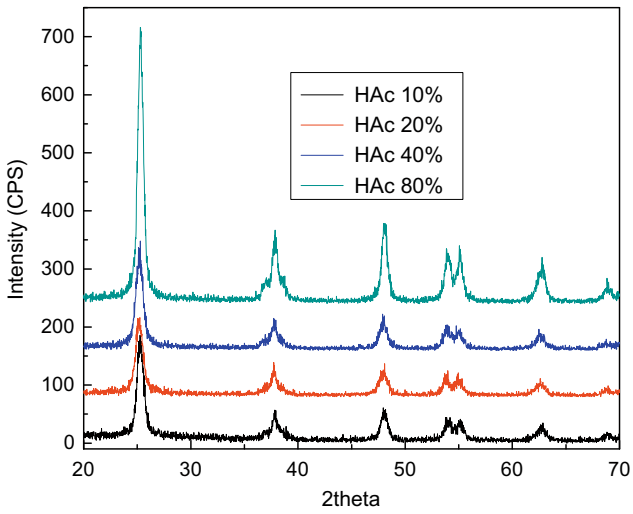

Fig. 1. XRD patterns of M-TiO_2 prepared in HAc-AS with different concentrations. (The hydrothermal treatment time, 48 h, and the calcination temperature 450 °C for 4 h.)

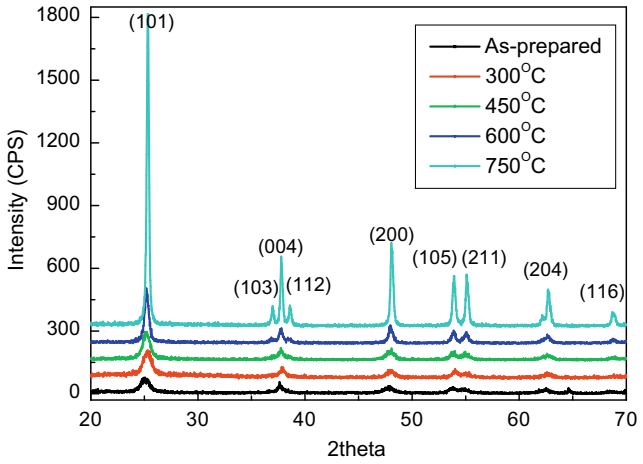

Fig. 2. XRD patterns of M-TiO_2 prepared at different calcination temperatures. (The acetic acid content, 20%, and the hydrothermal treatment time, 48 h.)

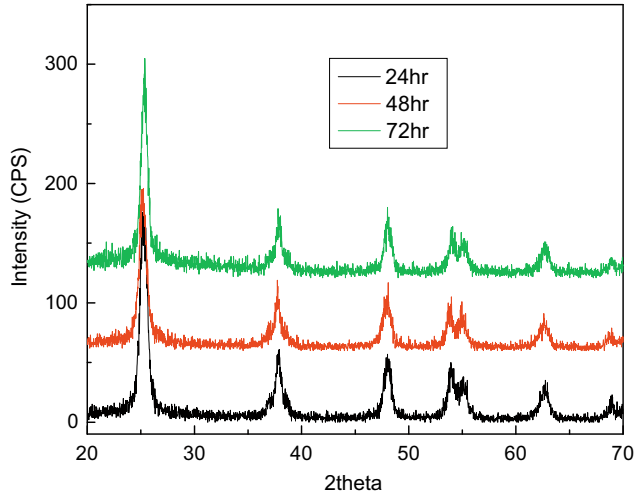

Fig. 3. XRD patterns of M-TiO_2 prepared at different hydrothermal treatment time. (The acetic acid content, 20%, and the calcination temperature 450 °C for 4 h.)

The gelation and condensation of organic titanium precursors involves the formation of Ti-OH and a further polymerization reaction of mononuclear complexes in order to form a polynuclear complex [38]. Polymeric titania hydrates will precipitate when the oligomeric Ti–O–Ti precursors grow to form a large size, which is called condensation. Because the rapid hydrolysis of titanium sources can be inhibited in HAc-AS due to the chelating effect and the acidity of HAc-AS, the hydrolysis rate of titanium sources decreases because the pH value of reaction solution decreases from 2.32 and 2.10 at the 10% and 20% HAc solution to 1.70 and 0.65 at 40% and 80% HAc solution. With decreasing the pH value, the hydrolysis of titanium sources was strongly inhibited. Therefore, the Ti–O–Ti species possesses a higher polymerization in order to precipitate in high-concentrated HAc-AS. Correspondingly, the crystalline sizes of the M-TiO_2 obtained in higher concentrated HAc-AS become larger, as indicated by Fig. 1.

The effect of calcination temperatures has been extensively studied due to its prominent effect on both the crystalline phase and the pore structure of resultant samples. Deduced from the XRD patterns shown in Fig. 2, with increasing the calcination temperature, the crystalline size of the M-TiO_2 remarkably increases from 10.5 to 31.8 nm. Moreover, we obtained the as-made sample of yellow agglomerates, yellow powders calcined at 300 °C, and lily powders calcined at 450, 600 and 750 °C. This is because there are many yellow P123 template existed in the as-made sample. However, after heat-treatment over 450 °C, most of yellow color template can be decomposed from the yellow agglomerates, and the colorless TiO_2 was finally obtained as only composition of the powder. The M-TiO_2 maintains the pure anatase phase at the calcination temperature as high as 750 °C, which indicates that the anatase in the obtained M-TiO_2 has very good phase stability.

Hydrothermal treatment has been widely employed as an efficient method to control the phase composition and the morphology of the products [39,40]. As shown in Fig. 3 and Table 1, the extension of the hydrothermal treatment time from 24 to 48 h leads to a slight increased crystalline size and the better pore structure of the M-TiO_2 products. However, if further increasing the hydrothermal treatment time to 72 h, the surface area decreases a little even if the crystalline size and the mean pore size gradually increase. Thus, we maybe can conclude that the 48 h is the best hydrothermal treatment time for preparing good M-TiO_2 products.

3.1.2. N_2 adsorption/desorption measurement

The N_2 adsorption/desorption isotherms and Barrett–Joyner–Halenda (BJH) pore size distributions of representative sample is displayed in Fig. 4. We can easily see from figure that the isotherm

Table 1
Structural parameters of M-TiO_2 prepared in different synthetic conditions.

Concentration of HAc-AS (%)	Calcination temperature (°C)	Time of hydrothermal treatment (h)	Crystalline size[a] (nm)	SBET[b] (m^2/g)	Mean pore size[c] (nm)	Total volume[d] (cm^3/g)
10	450	48	12.2	107	8.7	0.30
20	450	48	13.6	116	9.0	0.31
40	450	48	14.3	103	9.0	0.32
80	450	48	14.9	106	8.4	0.30
20	Not calcined	48	10.5	2	7.9	0.006
20	300	48	12.2	139	8.4	0.38
20	450	48	13.6	116	9.0	0.31
20	600	48	19.7	50	11.0	0.18
20	750	48	31.8	11	17.0	0.07
20	450	24	13.5	112	8.4	0.31
20	450	48	13.6	116	9.0	0.31
20	450	72	14.3	106	9.5	0.33

[a] Calculated by the Scherrer formula.
[b] BET surface area calculated from the linear part of the BET plot.
[c] Estimated using the desorption branch of the isotherm.
[d] Single-point total pore volume of pores at $P/P_0 = 0.99$.

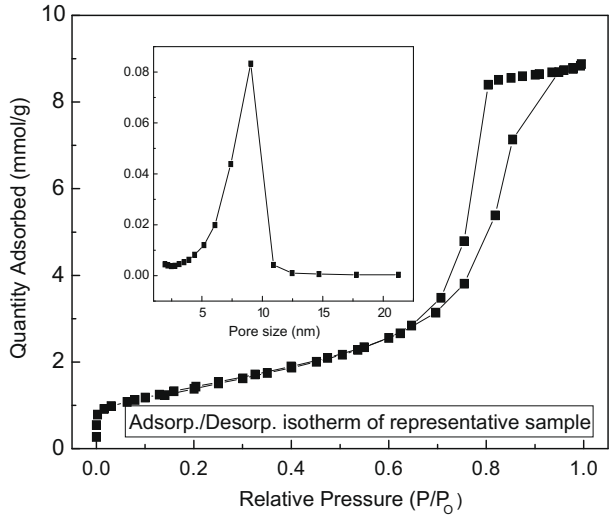

Fig. 4. N_2 adsorption/desorption isotherm and BJH pore size distribution of representative sample. (The acetic acid content, 20%, the hydrothermal treatment time, 48 h, and the calcination temperature 450 °C for 4 h.)

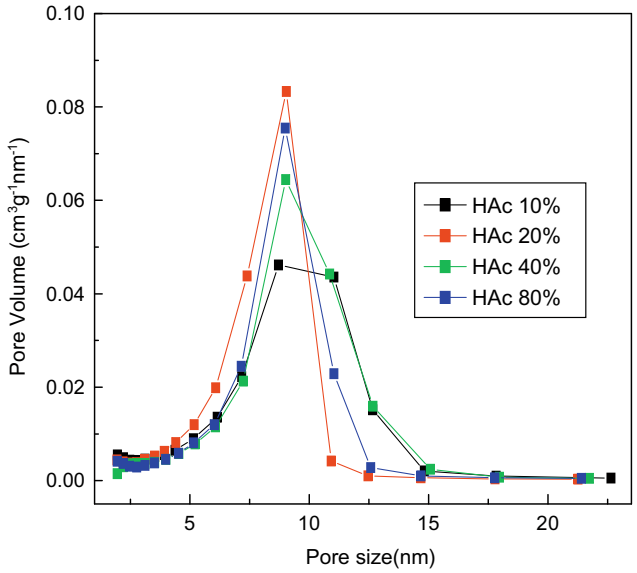

Fig. 5. BJH pore size distributions of M-TiO_2 prepared in HAc-AS with different concentrations. (The hydrothermal treatment time, 48 h, and the calcination temperature 450 °C for 4 h.)

is of type IV curve with a H1 hysteresis loop, which implies that the representative sample has ordered cylindrical pore geometry with a high degree of pore size uniformity with the average size of 9.0 nm [41,42]. The textural and structural parameters of the obtained samples have been summarized in Table 1. From the table, we can conclude that with increasing the concentration of HAc-AS, the BET surface area and the mean pore size of the products increase and then decrease, exhibiting a maximum surface area of 116 m^2/g, corresponding to mean porous size of 9.0 nm. The fluctuation may be attributed to the increasing molar ratio of H_2O/Ti with decreasing the concentration of HAc-AS, which is similar to those reported by Huang et al. [38] and Calleja et al. [43]. Meanwhile, we notice that the rapid hydrolysis of titanium butoxide occurred in 10% HAc aqueous solution, which further confirms the previous assumption that the increase of water content at the lower concentration can stabilize the complex polymer and leads to the formation of a well-developed structure. However, high water content seems lead to uncontrolled hydrolysis and condensation reaction, almost instantly giving TiO_2 precipitates, thus leading to poor chemical structure of TiO_2 materials [38]. Thus, the relatively broad pore size distribution of the M-TiO_2 obtained in 10% HAc-AS (shown in Fig. 5) may be aroused by the disordered arrangement of titanium oligomeric precursors. With increasing the concentration of HAc-AS to 20%, the apparent hydrolysis was also immediately observed when the $Ti(OC_4H_9)_4$ was titrated to the HAc-AS. However, after stirring for 4 h, the turbid solution gradually became transparent again and turned into a stable sol, which may be due to a kind of competitive relationship between the acetate groups and hydroxyl released by the ionization of water. When the concentration of acetate groups attains a certain value, acetate groups can replace both the butoxy of titanium butoxide and the hydroxyl which has already bonded to titanium sources. The M-TiO_2 prepared in 20% HAc-AS exhibits a narrow pore size distribution the same as that of the samples prepared in 40% and 80% HAc-AS. In 40% and 80% HAc-AS, no hydrolysis of titanium sources was observed throughout the titration and the aging time. Notably, the solation of titania condensation in 20% HAc-AS undoubtedly reflects that the strong chelating effect of HAc-AS plays a key role

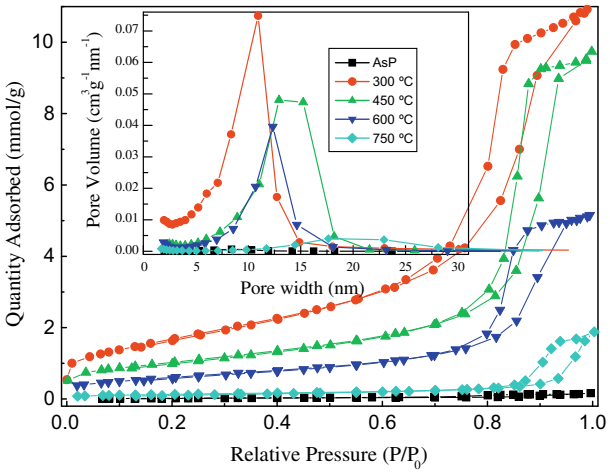

Fig. 6. N_2 adsorption/desorption isotherm and BJH pore size distribution of M-TiO_2 calcined at differential temperatures for 4 h. (The acetic acid content, 20%, the hydrothermal treatment time, 48 h.)

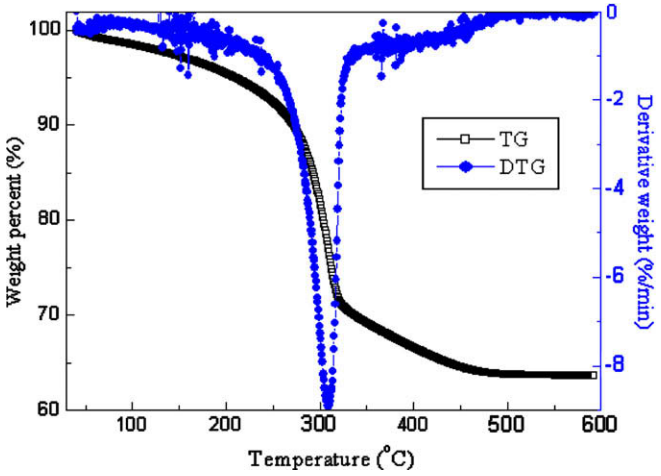

Fig. 7. Simultaneous TG and DTG curves for as-prepared TiO_2 sample. (The acetic acid content, 20%, and the hydrothermal treatment time, 48 h.)

in retarding the hydrolysis of titanium sources, which presents a new method to synthesize ordered mesostructured materials.

As shown in Table 1, both the mean pore size and the crystalline size increase monotonously with increasing the hydrothermal treatment time and the calcination temperature. The pore channels may be severely blocked by a large amount of surfactants remaining in the as-prepared samples. Therefore, the broader pore size and small pore volume can be observed in Fig. 6. For the as-prepared samples, the apparent excessive desorption occurs in the N_2 adsorption/desorption isotherm, which may be due to the extremely low surface area and small pore volume of as-prepared samples. Except for the as-prepared samples, with increasing the calcination temperature from 300 to 750 °C, the surface area and the pore volume decreased significantly, as well as the amount of adsorption N_2. But, both the crystalline size and the mean pore size of particles were increase gradually. These phenomena can be explained by fact that with increase the calcination temperature, the particle size would grow much large due to the physical aggregate of TiO_2 particles, leading to the significant decrease of the surface area and the pore volume of all the prepared samples, even if the mean pore size of particles was increased due to the rebuilding the pores of the TiO_2 materials. Excessive desorption and a broad pore size distribution (Fig. 6) appear again when the samples was calcined at 750 °C, which may be attributed to the collapsed mesoporous structure and disordered aggregation of bulky TiO_2 particles.

Such notable structural changes cannot be achieved by varying the concentration of HAc-AS and the hydrothermal treatment time. This indicates that a high calcination temperature can partly destroy the mesoporous structure of the obtained M-TiO_2. Moreover, the as-prepared sample exhibit a extremely low surface area and small pore volume, while the calcined samples exhibit a steep decrease of the surface areas and the pore volumes as the destruction of mesoporosity due to the high calcination temperatures, which indicate that the large surface area and the pore volume of the prepared M-TiO_2 is due to the formation of mesoporous structures. The simultaneous thermogravimetric (TG) and its time derivative (DTG) profiles were illustrated in the Fig. 7. From the figure, we can easily find that, with increase of the heat temperature, the mass loss curve (TG) decreased slowly before 200 °C, indicating the dehydration of the adsorbed water and the evaporation of acetic acid existed in the sample. At this stage, the prepared material has 5% weight loss. However, after this temperature, the mass loss enhanced very fast (23.534% weight loss) until the temperature arrived at the temperature of 318 °C, and it reaches the highest rate of mass losses (DTG) at around 309 °C. This significant drop is mainly contributed to the combustion of the template P123. Thus we can conclude that most of the template P123 can completely decompose at 309 °C. However, after this stage, another 10.5% mass loss was also obtained, lasting a long interval of 200 °C. This slowly drops of mass loss maybe due to the slight change of the morphology of prepared M-TiO_2. As shown in Table 1, with increasing the calcination temperature from 300 °C, the surface area and the pore volume of the obtained M-TiO_2 decrease slowly first before 450 °C and then declined rapidly after the temperature of 600 °C, which indicates that the mesoporous structure is stable below 450 °C.

3.1.3. Surface morphology of the prepared M-TiO_2

As for the M-TiO_2 prepared in different HAc-AS and at different hydrothermal treatment time, the crystalline size exhibits slight change as indicated by the XRD patterns. The TEM image of the as-prepared samples is unavailable because of a large amount of residual surfactants. Therefore, only the images of the M-TiO_2 prepared at different calcination temperatures are presented here. As shown in the TEM images (Fig. 8), the samples consist of the aggregation of nanoparticles with particle sizes of 10–40 nm. The particle size increases apparently with increasing the calcination temperature, agreeing with the results calculated from the XRD patterns. Long-range ordered mesoporous structures were not observed in the TEM images and the mesoporosity is mainly due to the interparticle porosity rather than intraparticle porosity, which is consistent with the lack of diffraction peaks at the small-angle XRD pattern (not shown here). Therefore, the aggregation of nanoparticles is supposed to be the main reason of the formation of mesostructures.

3.2. Photocatalytic activity of M-TiO_2

The photocatalytic activity of the obtained M-TiO_2 was assessed using DMP as a model compound. The photocatalytic degradation curves of DMP are presented in Figs. 9–12. As shown in Fig. 9,

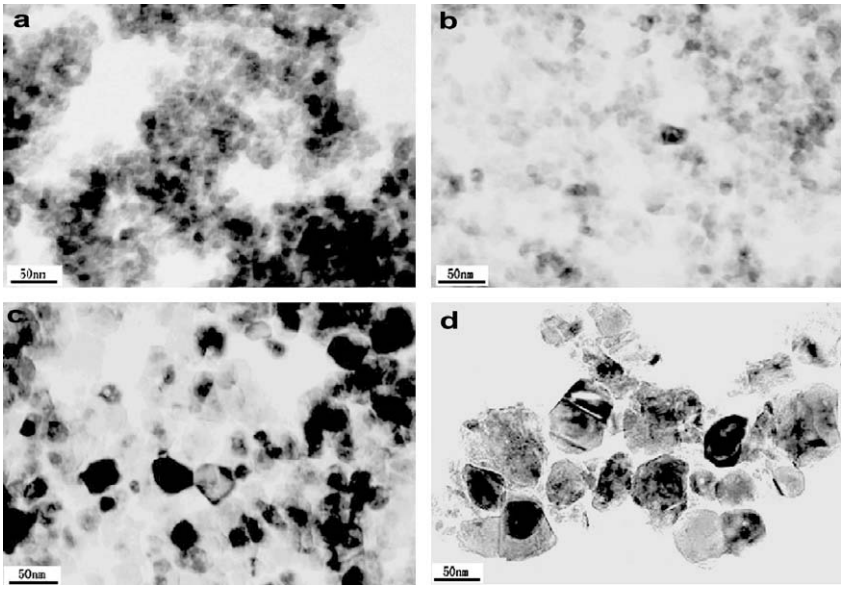

Fig. 8. TEM images of M-TiO_2 prepared at different calcination temperatures: a: 300 °C; b: 450 °C; c: 600 °C; and d: 750 °C. (The acetic acid content, 20%, and the hydrothermal treatment time, 48 h.)

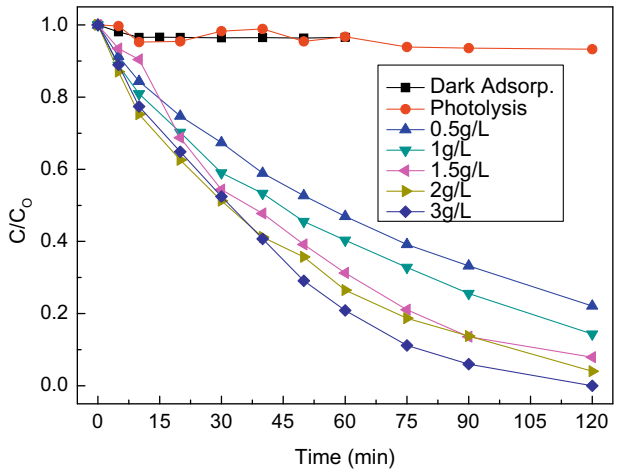

Fig. 9. Dark adsorption and photocatalytic degradation curves of DMP over different photocatalyst concentration. (The initial concentration of DMP, 2.5×10^{-4} mol/L.)

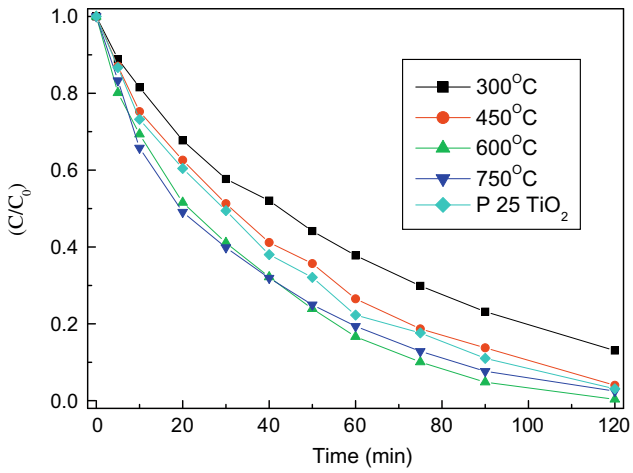

Fig. 11. Degradation curves of DMP using M-TiO_2 photocatalysts prepared at different calcination temperatures.

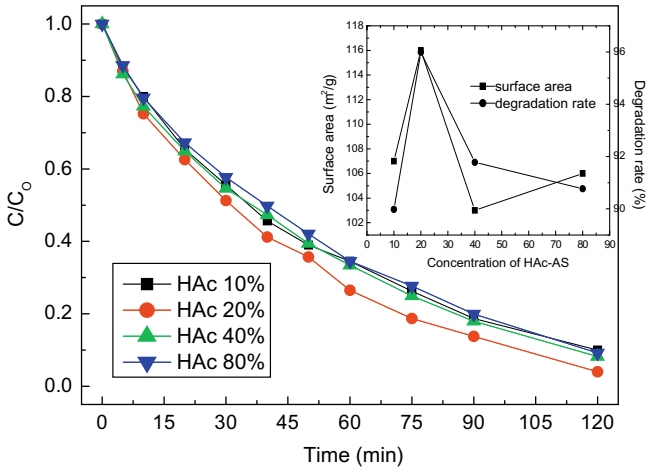

Fig. 10. Degradation curves of DMP using M-TiO_2 photocatalysts prepared in HAc-AS with different concentrations.

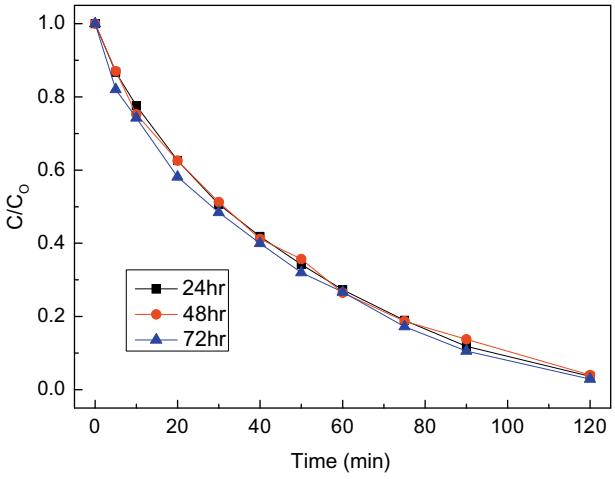

Fig. 12. Degradation curves of DMP using M-TiO_2 photocatalysts prepared at different hydrothermal treatment time.

the removal efficiencies of dark adsorption and the photolysis of DMP are 3.48% and 6.75%, respectively. The low adsorption of the obtained M-TiO_2 may be attributed to the hydrophobicity of DMP and the hydrophilicity of M-TiO_2. A low photodegradation efficiencies of DMP further confirms its high stability under UV-light. However, with the addition of only 0.5 g/L representative M-TiO_2 sample, the degradation efficiency increases remarkably to 77.88%. With increasing the amount of photocatalysts, the degradation efficiencies gradually increases up to 100% with 3 g/L representative sample. As the concentration of photocatalysts increases above 1.5 g/L, the degradation efficiencies of DMP increases slowly, which may be ascribed to the shielding effect of the excessive M-TiO_2 on UV-light. Thus, the optimal 2 g/L concentration of photocatalysts was used for all the other three contrastive experiments.

Fig. 10 presents the degradation efficiencies of DMP using the M-TiO_2 prepared in different concentrations of HAc-AS. Photocatalytic activity of the M-TiO_2 is strongly dependent on the phase structure, crystalline size, surface area and pore structure [44]. From the inset to Fig. 10, the curves show the agreeable changing trend for both the photocatalytic activity and the surface area of the M-TiO_2, which indicates that the surface area is the dominant effect in this contrastive group. In Fig. 11, it can be observed that with increasing the calcination temperatures from 300 to 450 °C, the photocatalytic activity of the obtained M-TiO_2 is improved apparently. As previous illustration, the surfactants can be efficiently burned out with increasing the calcination temperature below 450 °C. Meanwhile, the anatase phase with good crystallinity can be obtained by calcination over 450 °C. The improved anatase phase structure contributes to the enhanced photocatalytic activity of the M-TiO_2 obtained by calcination at 600 °C. However, larger crystalline size, lower surface area and smaller pore volume are considered to have negative effects on the photocatalytic activity [45]. Increasing the calcination temperature from 450 to 600 °C brings trivial increase of the degradation efficiencies of DMP (3.64%). And a slightly decreased degradation efficiencies of DMP was also observed over the samples calcined at 750 °C, which may be ascribed to the collapse of mesoporous structure, resulting in severe decrease of the surface area and the pore volume of M-TiO_2. Known from the above results, we concluded that the phase structure as well as the surface area of the prepared M-TiO_2 possessed the dominant effect on the photocatalytic activity of the samples. The photocatalytic degradation efficiencies of Degussa P25 TiO_2 were also carried out and compared with the other degradation data shown in Fig. 11. Seen from the figure, the photocatalytic efficiency of P25 TiO_2 is slight higher than that of the M-TiO_2

calcined at 450 °C, but a little lower than that of M-TiO_2 calcined at 750 °C as well as 600 °C. The higher photocatalytic efficiencies of the M-TiO_2 calcined at 600 °C as well as 750 °C can be attributed to the pure and good anatase phases which still keep at the higher calcination temperature as high as 750 °C.

Fig. 12 shows the photocatalytic degradation curves of DMP over the M-TiO_2 prepared at different hydrothermal treatment time. The degradation efficiencies of DMP over the M-TiO_2 prepared with hydrothermal treatment for 24, 48 and 72 h are 96.4%, 96.0% and 97.1%, respectively. Generally, the photocatalytic activity changes slightly because of the unremarkable diversity of phase structure, surface area and pore volume.

Under the same reaction condition, the intrinsic characteristics of photocatalysts have a complex effect on the ultimate photocatalytic activity. According to our research, we can reliably conclude that the phase structure, surface area and pore volume have notable effects on the photocatalytic activity of M-TiO_2. The crystalline size and mean pore size of M-TiO_2 may have a certain effect on the photocatalytic activity. A recent review [46] has also pointed out that satisfying explanations on why the ordered mesoporous materials are superior to less ordered catalysts are still lacking.

4. Conclusions

Acetic acid aqueous solution was used as both hydrolytic retardants and acid catalysts to successfully prepare mesoporous TiO_2 nanomaterials with large mean pore sizes and narrow pore size distributions under hydrothermal condition. The rapid hydrolysis of titanium sources has been efficiently controlled using a low concentrated acetic acid aqueous solution (20% v/v). Especially, the condensed TiO_2 are found to solate in 20% acetic acid aqueous solution, which is due to the strong chelating effect of acetic acid. The obtained mesoporous anatase TiO_2 exhibit good thermal stability. The crystal phase and the pore structures of the obtained mesoporous TiO_2 are tunable by changing the synthetic conditions, such as the concentration of acetic acid, calcination temperature and hydrothermal treatment time. TEM images reveal that the formation of mesostructures is probably due to the effective aggregation of TiO_2 nanoparticles directed by the Pluronic P123 template. The prepared mesoporous TiO_2 possesses good activity for the photocatalytic degradation of a kind of representative persistent organic pollutants – dimethyl phthalate. The phase structure, the surface area and the pore volume have notable effects on the photocatalytic activity of the prepared mesoporous TiO_2, comparable to the effects of the crystalline size and the mean pore size.

Acknowledgments

This is contribution No. IS-1082 from GIGCAS. This work was financially supported by the national Natural Science Foundation of China (40572173 and 40302013) and the Science and Technology Project of Guangdong province, China (2007A032301002 and 2006A36701002).

References

[1] C.T. Kresge, M.E. Leonowicz, W.J. Roth, J.C. Vartuli, J.S. Beck, Nature 359 (1992) 710.
[2] J.S. Beck, J.C. Vartuli, W.J. Roth, M.E. Leonowicz, C.T. Kresge, K.D. Schmitt, C.T.W. Chu, D.H. Olson, E.W. Sheppard, S.B. Mc-Cullen, J.B. Higgins, J.L. Schlenker, J. Am. Chem. Soc. 114 (1992) 10834.
[3] T. Maschmeyer, F. Rey, G. Sankar, J.M. Thomas, Nature 378 (1995) 159.
[4] O.A. Kholdeeva, N.N. Trukhan, M.P. Vanina, V.N. Romannikov, V.N. Parmon, J. Mrowiec-Bialon, A.B. Jarzebski, Catal. Today 75 (2002) 203.
[5] V. Parvulescu, C. Anastasescu, C. Constantin, B.L. Su, Catal. Today 78 (2003) 477.
[6] M. Raimondo, G. Perez, M. Sinibaldi, A.D. Stefanis, A.A.G. Tomlinson, Chem. Commun. (1997) 1343.
[7] H. Hata, S. Saeki, T. Kimura, Y. Sugahara, K. Kuroda, Chem. Mater. 11 (1999) 1110.
[8] K. Kageyama, S. Ogino, T. Aida, T. Tatsumi, Macromolecules 31 (1998) 4069.
[9] Z. Peng, Z. Shi, M. Liu, Chem. Commun. (2000) 2125.
[10] M.R. Hoffmann, S.T. Martin, W. Choi, D.W. Bahnemann, Chem. Rev. 95 (1995) 69.
[11] D.M. Antonelli, J.Y. Ying, Angew. Chem., Int. Ed. 34 (1995) 2014.
[12] K.S. Yoo, T.G. Lee, J. Kim, Micropor. Mesopor. Mater. 84 (2005) 211.
[13] L. Zhao, Y. Yu, L. Song, M. Ruan, X. Hu, A. Larbot, Appl. Catal. A 263 (2004) 171.
[14] M.H. Lim, C.F. Blanford, A. Stein, J. Am. Chem. Soc. 119 (1997) 4090.
[15] H. Yang, N. Coombs, G.A. Ozin, Nature 386 (1997) 692.
[16] G.S. Attard, J.C. Glyde, C.G. Göltner, Nature 378 (1995) 366.
[17] P.T. Tanev, T.J. Pinnavaia, Science 267 (1995) 865.
[18] R. Mokaya, W. Zhou, W. Jones, Chem. Commun. (1999) 51.
[19] D. Zhao, Q. Huo, J. Feng, B.F. Chmelka, G.D. Stucky, J. Am. Chem. Soc. 120 (1998) 6024.
[20] Z. Luan, C. Cheng, W. Zhou, J. Klinowski, J. Phys. Chem. 99 (1995) 1018.
[21] A. Monnier, F. Schuth, Q. Huo, D. Kumar, D. Margolese, R.S. Maxwell, G.D. Stucky, M. Krishnamurty, P. Petroff, A. Firouzi, M. Janicke, B.F. Chmelka, Science 261 (1993) 1299.
[22] Q. Huo, D.I. Margolese, U. Ciesla, D.G. Demuth, P. Feng, T.E. Gier, P. Sieger, A. Firouzi, B.F. Chmelka, F. Schuth, G.D. Stucky, Chem. Mater. 6 (1994) 1176.
[23] P. Yang, D. Zhao, D.I. Margolese, B.F. Chmelka, G.D. Stucky, Nature 396 (1998) 152.
[24] G.J.d.A.A. Soler-Illia, A. Louis, C. Sanchez, Chem. Mater. 14 (2002) 750.
[25] E.L. Crepaldi, G.J.d.A.A. Soler-Illia, D. Grosso, F. Cagnol, F. Ribot, C. Sanchez, J. Am. Chem. Soc. 125 (2003) 9770.
[26] F. Kleitz, L.A. Solovyov, G.M. Anilkumar, S.H. Choi, Chem. Commun. (2004) 1536.
[27] S.Y. Choi, M. Mamak, N. Coombs, N. Chopra, G.A. Ozin, Adv. Funct. Mat. 14 (2004) 335.
[28] T.-W. Kim, F. Kleitz, B. Paul, R. Ryoo, J. Am. Chem. Soc. 127 (2005) 7601.
[29] D. Zhao, J. Feng, Q. Huo, N. Melosh, G.H. Fredrickson, B.F. Chmelka, G.D. Stucky, Science 279 (1998) 548.
[30] M. Zhang, T. An, X. Hu, C. Wang, G. Sheng, J. Fu, Appl. Catal. A 260 (2004) 215.
[31] C. Wang, Z. Deng, Y. Li, Inorg. Chem. 40 (2001) 5210.
[32] E. Stathatos, P. Lianos, C. Tsakiroglou, Micropor. Mesopor. Mater. 75 (2004) 255.
[33] H. Choi, E. Stathatos, D.D. Dionysiou, Thin Solid Films 510 (2006) 107.
[34] S. Doeuff, M. Henry, C. Sanchez, J. Livage, J. Non-Cryst. Solids 89 (1986) 206.
[35] D.P.B. III, N.J. Bendzko, Mater. Chem. Phys. 59 (1999) 26.
[36] J.C. Yu, L. Zhang, J. Yu, New J. Chem. (2002) 416.
[37] H.P. Klug, L.E. Alexander (Eds.), X-ray Diffraction Procedures for Polycrystalline and Amorphous Materials, Wiley, New York, 1974.
[38] D. Huang, G.S. Luo, Y.J. Wang, Micropor. Mesopor. Mater. 84 (2005) 27.
[39] C. Su, C.-M. Tseng, L.-F. Chen, B.-H. You, B.-C. Hsu, S.-S. Chen, Thin Solid Films 498 (2006) 259.
[40] G. Wang, J. Mol. Catal. A: Chem. 274 (2007) 185.
[41] M. Kruk, M. Jaroniec, Chem. Mater. 13 (2001) 3169.
[42] T.C. An, J.K. Liu, G.Y. Li, S.Q. Zhang, H.J. Zhao, X.Y. Zeng, G.Y. Sheng, J.M. Fu, Appl. Cal. A: General. 350 (2008) 237.
[43] G. Calleja, D.P. Serrano, R. Sanz, P. Pizarro, A. Garcia, Ind. Eng. Chem. Res. 43 (2004) 2485.
[44] B. Wen, C. Liu, Y. Liu, J. Photochem. Photobio. A: Chem. 173 (2005) 7.
[45] J.C. Yu, J. Yu, L. Zhang, W. Ho, J. Photochem. Photobio. A: Chem. 148 (2002) 263.
[46] A. Taguchi, F. Schuth, Micropor. Mesopor. Mater. 77 (2005) 1.